Splitting of resonant Raman x-ray peaks near the M_{IV} and M_V edges of uranium

G. E. Ice

Metals and Ceramics Division, Oak Ridge National Laboratory, Oak Ridge, Tennessee 37831

E. Isaacs

AT&T Bell Laboratories, Murray Hill, New Jersey 07974

P. Zschack

Oak Ridge Associated Universities, Oak Ridge, Tennessee 37830

(Received 2 October 1991; revised manuscript received 2 October 1992)

Resonant Raman x-ray-scattering spectra have been measured at 1 eV resolution with the incident x-ray energy tuned near the uranium M_{IV} and M_V absorption edges. Measurements were made on a single crystal of URu_2Si_2. Inelastic x-ray spectra were collected within ± 30 eV of the U $M_{IV}(3d\ \frac{3}{2})$-$N_{VI}(4f\ \frac{5}{2})$ and the U $M_V(3d\ \frac{5}{2})$-$N_{VII}(4f\ \frac{7}{2})$ x-ray-emission lines. The incident beam was tuned through the M_{IV} and M_V threshold energies. At both edges the emission spectra are dominated by three lines: a diagram line (corresponding to the promotion of an electron to the continuum), a large spectator line (arising from the promotion of an electron into a pre-edge band), and a smaller companion spectator line. The spectator lines exhibit linear dispersion as a function of the incident x-ray energy and the spectator lines have resonances ~ 4 eV below the continuum thresholds. At the U M_{IV} edge, the large spectator line is assigned to the M_{IV}-N_{VI} transition. The small spectator line has an x-ray energy about 7 eV higher, which is 3 eV below the forbidden M_{IV}-N_{VII} line. At the U M_V edge the main spectator line is assigned to the M_V-N_{VII} transition with a smaller peak 10 eV lower near the M_V-N_{VI} position. The intensity of the small M_V spectator line relative to the M_V-N_{VII} spectator line is much larger than the diagram line ratio of M_V-N_{VI}/M_V-N_{VII} observed with nonresonant electron-excited spectra. The emission spectra were corrected for resonance enhancement to study the coupling of the $3d(\frac{3}{2})$ and $3d(\frac{5}{2})$ electrons to the near-edge density of unoccupied states. The near-edge, or "white-line," feature at the M_V edge is found to be flat topped, while the near-edge feature at the M_{IV} edge is asymmetric and peaked.

INTRODUCTION

The recent availability of synchrotron radiation now makes it possible to study emission spectra with the incident x-ray energy tuned near threshold. Here, we report the measurement of uranium M x-ray-emission spectra with the incident energy tuned near threshold, in contrast to previous measurements made far above threshold.[1-5] This measurement is timely, since interest in threshold uranium M x-ray emission spectra has been stimulated by the discovery of enormous x-ray resonant-magnetic-scattering cross sections near the U M_{IV} and M_V edges.[6] These large cross sections arise primarily from electric-dipole transitions and are a consequence of spin splitting associated with local moments.[7] With this enhanced x-ray scattering, it has been possible to make uniquely sensitive measurements of magnetic ordering in uranium heavy-fermion compounds,[6,8,9] yet some details of the observed resonances are not fully understood. For example, theoretical estimates are in rough agreement with the size of the observed U M_{IV} resonance, but are high by a factor of 10 for the M_V resonance.[9] Also, there is surprising uniformity in the energy dependence of the enhancement observed for different U compounds, even though the peak enhancement scales with the square of the magnetic moment.[8-10]

To help in understanding the details of the uranium M-edge x-ray magnetic-resonance scattering (XMRS), we have undertaken a measurement of the x-ray-emission spectra excited near the M_{IV} and M_V edges. Measurements of near M-edge x-ray-emission spectra are relevant because, as described below, both processes are sensitive to the same matrix elements. No other technique can study the spectroscopy of XMRS with such detail. Absorption-edge measurements, although sensitive to the same matrix elements, have resolutions limited by the lifetime-broadened hole width of the edge hole. This limitation can be removed either by measuring the emission spectra over a narrow band as the incident beam is tuned[11] or by measuring the entire spectra as described here. Measurement of the entire spectra is preferred, as illustrated by this experiment, because changes in matrix elements and emission multiplet structure near an edge can be detected. The measurements described below are of sufficient resolution to begin to study details of the unfilled density of states to which the core-hole electron is promoted. The density of unfilled states can also be measured by bremsstrahlung isochromat spectroscopy (BIS), but this technique is insensitive to wave-function symmetry and atomic species.[12]

Near an absorption edge, x-ray-emission spectra are best described in terms of the x-ray resonant Raman-

scattering (XRRS) formalism.[13,14] X-ray resonant Raman scattering was first recognized by Sparks[15] using conventional sealed x-ray tubes. Sparks discovered that a relatively strong inelastic scattering peak remained near the characteristic fluorescence lines when the incident x-ray energy was not too far below threshold. The peak intensity increased rapidly as Z was varied to cause the K threshold to approach the incident x-ray energy. Theoretical discussions of XRRS have been given by Nozières and Abrahams,[16] Gravilla and Tugulea,[17] and by Bannet and co-workers.[18,19]

A detailed experimental study of XRRS in Cu was made by Eisenberger, Platzman, and Winick[20,21] using synchrotron radiation. This work confirmed the Sparks results, and demonstrated two of the remarkable features of XRRS: (i) linear dispersion of the XRRS line with incident energy, and (ii) emission line width narrower than the inner shell hole lifetime width. A theoretical description that emphasizes the relationship between XRRS and anomalous x-ray scattering, first pointed out by Sparks,[15] has been given by Suortti.[22,23] This work also discusses the potential application of XRRS for studying the density of unfilled states. A paper that reports measurements of K-M XRRS and discusses possible applications has been given by Kodre and Shafroth.[24] Recent theoretical discussions have been given by Tulkii and Åberg.[25]

A particularly interesting recent result was the

discovery of an Auger analog to XRRS by Brown et al.[26] They observed splitting of the Auger multiplet lines due to the structure in the unfilled density of states to which the inner shell hole electron couples. The measurements were made on xenon gas, which allowed for a simple interpretation of the observed structures in terms of atomic states. Subsequent measurements have been made on Argon.[27,28] Also of interest have been measurements of polarization anisotropy in x-ray emission from molecules[29,30] and measurements of screening shifts in molecular gases.[31] These measurements demonstrate the sensitivity of x-ray emission to the atomic or molecular structure in the density of states when excited near threshold. Particularly relevant are observed shifts in emission lines associated with the promotion of an inner shell electron to a bound excited state. Analogous and even more dramatic changes in the radiationless emission spectra have been observed when a bound-state resonance is excited in Be[32] and Mg[33].

THEORY

To help in interpreting the results of our measurements, we briefly review the theory of resonant x-ray scattering. This section closely follows the notation and development of Refs. 20–23. In the nonrelativistic limit, x-ray scattering to second order is described by the modified Kramers-Heisenberg formula:[34]

$$\left[\frac{d^2\sigma}{d\omega_2 d\Omega}\right]_{AB} = r_0^2 \left[\frac{\omega_2}{\omega_1}\right] \left|\langle B|e^{i\mathbf{k}\cdot\mathbf{r}}|A\rangle(\mathbf{e}_1\cdot\mathbf{e}_2) - \frac{1}{m}\sum_I \left[-\frac{\langle B|\mathbf{p}\cdot\mathbf{e}_2|I\rangle\langle I|\mathbf{p}\cdot\mathbf{e}_1|A\rangle}{E_I - E_A - \hbar\omega_1 - i\Gamma_I/2} + \frac{\langle B|\mathbf{p}\cdot\mathbf{e}_1|I\rangle\langle I|\mathbf{p}\cdot\mathbf{e}_2|A\rangle}{E_I - E_A - \hbar\omega_2}\right]\right|^2$$

(1)

Here, r_0 is the electron radius, ω_1 and ω_2 are the incident and final photon frequencies, $d\Omega$ is the solid angle, $\mathbf{k}=\mathbf{k}_1-\mathbf{k}_2$ is the momentum transfer, and $\mathbf{e}_1$ and $\mathbf{e}_2$ are the polarization vectors of the incident and scattered radiation. E_A and E_B are the energies of the initial and final electron states, ($\langle A|,\langle B|$), I refers to an intermediate state, ($\langle I|$) and Γ_I is the lifetime width of the intermediate state. The term with the $\mathbf{e}_1\cdot\mathbf{e}_2$ polarization dependence is the well-known A^2 term. The ($\mathbf{A}\cdot\mathbf{P}$)^2 contribution is contained in the final two terms, of which the part with the complex denominator describes resonant scattering. As will be shown below, Eq. (1) describes the relationship between XRRS and anomalous x-ray scattering. Although Eq. (1) does not include magnetic-scattering terms explicitly,[35] magnetic order can be detected due to local differences in the anomalous scattering correction due to spin splitting.[7]

Far from threshold, the ($\mathbf{A}\cdot\mathbf{P}$)^2 contribution to the scattering cross section is negligible[36] and the first term dominates for both elastic and inelastic scattering. For elastic scattering $\langle A|=\langle B|$, and the first term leads to the well-known x-ray scattering form factor. If inelastic scattering is included, the first term leads to the dynamic scattering factor.[37]

In the case of resonant scattering, the incident photon

energy $\hbar\omega_1$ is nearly equal to the energy difference $E_I - E_A$. Here, the denominator of the resonant term becomes small, and the second term in Eq. (1) makes a significant contribution to the scattering. For elastic scattering, the resonant ($\mathbf{A}\cdot\mathbf{P}$)^2 term describes the anomalous dispersion corrections to the x-ray-scattering factor.[23] X-ray magnetic-resonance scattering is a special case of anomalous x-ray scattering.[6-8]

Resonant Raman scattering is described by Eq. (1) when near resonance, the intermediate state relaxes by x-ray emission, leaving the atom in an excited state. This process is illustrated in Fig. 1 for uranium M-N XRRS. We consider the case where the resonant term dominates. In a one-electron atomic model, the initial state $|A\rangle$ is the ground state of the atom. The intermediate state $|I\rangle$ refers to an atomic core hole ($3d$) with an electron promoted to a pre-edge band or to the continuum. The final state has a higher-lying core hole ($4f$) with the initially promoted electron remaining in its excited state. It is convenient to approximate the initial, final, and intermediate states by the product of one-electron states (e.g., $\langle I|=\langle 1s|^2\langle 2s|^2\langle 2p|^6\langle\cdots\rangle$). The matrix elements $\langle B|\mathbf{p}\cdot\mathbf{e}_2|I\rangle$ and $\langle I|\mathbf{p}\cdot\mathbf{e}_1|A\rangle$ are then given by $\langle 4f|\mathbf{p}\cdot\mathbf{e}_2|3d\rangle$ and $\langle k|\mathbf{p}\cdot\mathbf{e}_1|3d\rangle$. Here, the state $\langle k|$ is a band or continuum state with energy ϵ_k. This simplified

picture neglects correlation and relaxation effects.

Further simplification can be obtained by assuming that the matrix elements (M^2) vary slowly near resonance. This approximation is valid away from Cooper minima.[38] Representing the sum over intermediate states by an integral over the excited state $\langle k |$, using the requirement of energy conservation and assuming incoherent addition of the intermediate states, we find

$$\frac{d^2\sigma}{d\omega_2 d\Omega} \sim C \left| \frac{\omega_2}{\omega_1} \right| M^2 \int \frac{\eta(\epsilon_k)\delta(\hbar\omega_1 - \hbar\omega_2 - E_{4f} - \epsilon_k)d\epsilon_k}{(\hbar\omega_1 - \epsilon_k - E_{3d} + i\Gamma_{3d}/2)^2} ,$$ (2)

where $M = \langle 4f | \mathbf{p} \cdot \mathbf{e}_2 | 3d \rangle \langle k | \mathbf{p} \cdot \mathbf{e}_1 | 3d \rangle$. Here, E_{3d} and E_{4f} are the ionization energies of the $3d$ and $4f$ electrons and $\eta(\epsilon)$ is the density of unoccupied excited states at ϵ_k. The δ function in Eq. (2) imposes a one-to-one correspondence between the energy ϵ_k and the emission energy $\hbar\omega_2$ for incident x-ray energy $\hbar\omega_1$. Performing the integral in Eq. (2) and solving for η, we find

$$\eta(\epsilon_k = \hbar\omega_1 - \hbar\omega_2 - E_{4f})$$

$$\propto \frac{d^2\sigma}{d\omega_2 d\Omega} [(\hbar\omega_2 + E_{4f} - E_{3d})^2 - (\Gamma_{3d}/2)^2] .$$ (3)

Equations (2) and (3) have a simple interpretation. The inelastic x-ray-scattering cross section near the M-N emission line is very nearly modeled by the product of three functions of $\hbar\omega_2$. The first function is slowly varying and contains the matrix elements M^2 and some constants. The second function is a Lorentzian centered at $\hbar\omega_2 = (E_{3d} - E_{4f})$ with a width Γ_{3d}. The product of these first two functions looks spectroscopically like ordinary fluorescence. The third function is proportional to the density of states $\eta(\epsilon_k)$, where $\epsilon_k = \hbar\omega_1 - \hbar\omega_2 - E_{4f}$. Far above threshold, $\eta(\epsilon_k)$ is featureless, and the emission spectra takes on the fluorescent form. Near threshold, $\eta(\epsilon_k)$ may have a structure that exhibits linear dispersion with $\hbar\omega_1$. Sensitivity to $\eta(\epsilon_k)$ is greatest when $\hbar\omega_2$ is near the resonant peak $E_{3d} - E_{4f}$. This occurs when $\hbar\omega_1 = \epsilon_k + E_{3d}$. XMRS has the same $\langle k | \mathbf{p} \cdot \mathbf{e} | 3d \rangle$ matrix element and is also sensitive to the density of states $\eta(\epsilon)$.

EXPERIMENT

General

The experiment was performed on the Oak Ridge National Laboratory beamline $X14$ at the National Synchrotron Light Source (NSLS).[39] A schematic of the experimental setup is shown in Fig. 2. A platinum-coated x-ray mirror 7.5 m from the source focused the vertical beam divergence and acted as a low-pass filter.[40] The mirror angle was set to 6×10^{-3} rad to efficiently collect the vertical divergence at 3.7 keV, and to absorb x rays above 10 keV. A two-crystal Si(111) sagittal-focusing monochromator located 9.2 m from the source focused 4.5×10^{-3} rad of horizontal divergence onto the sample. The monochromator was tuned to pass a narrow band near the M_{IV} and M_V uranium edges at 3.728 and 3.552 keV.

The sample was a single crystal of URu_2Si_2 located in a cryostat at the center of a six-circle diffractometer 19 m from the source. The x-ray-emission spectrum was measured using a mosaic graphite (002) monochromator.[41] The graphite crystal had a mosaic spread of 0.8 degrees, and a sagittal radius of 10 cm. The source to monochro-
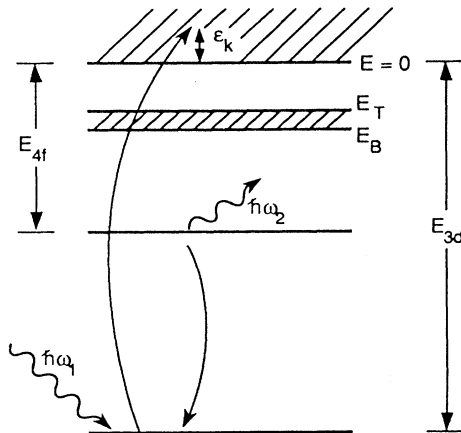

FIG. 1. Schematic of the energy levels for uranium M-N x-ray resonance Raman scattering. ϵ_k is the energy of the electron promoted from the core. E_{3d} and E_{4f} are the $3d$ and $4f$ binding (or threshold) energies. $\hbar\omega_1$ and $\hbar\omega_2$ are incident and emission x-ray energies.
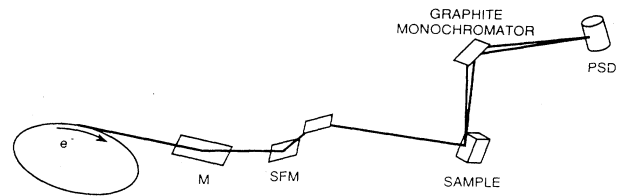

FIG. 2. Experimental design at the Oak Ridge National Laboratory beamline X14 at the NSLS. The synchrotron radiation is generated at a bending magnet on the NSLS x-ray ring. The vertical divergence is focused by a mirror labeled M. The horizontal divergence is focused by a sagittally focusing crystal in the two-crystal Si(111) monochromator labeled SFM. The focused and monochromated beam impinges on the URu_2Si_2 single crystal normal to the surface. The emission spectra are observed at a 10-degree takeoff angle using a graphite (002) monochromator that parafocuses onto a linear-position-sensitive detector.

mator distance was 59 cm. In this geometry, the mosaic crystal was overfocused sagittally, limiting the useful crystal width to about 2 mm. The detector was located for unit magnification at 59 cm from the graphite crystal. The emission spectra was parafocused onto the linear detector by the mosaic crystal.[41] Because of severe absorption losses in air, all flight paths were either in vacuum or helium. Windows were also minimized to preserve flux.

Energy resolution

The X14 line is well matched to this experiment. Compared to the more common separate-function design,[42] there is very little mixing of the horizontal and vertical beam divergences.[43] As a result, the energy resolution is not degraded by horizontal acceptance, and the incident energy resolution can be estimated as for a simple two-crystal monochromator. The rms unfocused beam divergence from the NSLS at 3.7 keV (U M_{IV}) is estimated to be $\sim 1.2 \times 10^{-4}$ rad. Because the mirror is magnifying,[44] the divergence after the mirror is around 7.5×10^{-5} rad. This yields a full-width-at-half-maximum (FWHM) energy bandpass $(dE = E \cot\theta \, d\theta)$ of 1.1 eV. The energy spread at the U M_V edge should be slightly smaller.

For a Raman experiment, both the incident and the scattered x-ray energy must be accurately measured. The energy resolution of the graphite monochromator was limited predominantly by the effective source size. This is because the parafocusing monochromator projected a one-to-one monochromatic image of the source onto the linear detector. To achieve small effective source size, the incident beam was slit to 1–2 mm. This gives a FWHM beam size of 0.7–1.4 mm. The vertical focus at X14 is approximately 1 mm, but the position can drift due to beam-orbit instabilities. The slit, therefore, insured a minimum source size during a long scan. The incident beam was allowed to impinge normal to the sample surface (Fig. 2). The detector optics were then aligned at 10 degrees to the surface. In this asymmetric geometry there is a $5\times$ demagnification in the effective source size to ~ 0.12–0.23 mm. The FWHM resolution can then be determined from the source-size resolution formula for a mosaic crystal $dE = (ES \cot\theta)/2F_1$.[41] Here, S is the source size, F_1 is the crystal to detector distance, and θ is the Bragg angle. For the present experiment, the source-size resolution was estimated to be 0.35–0.7 eV. The emission-spectra resolution convoluted from all causes was estimated to be less than 0.8–1.0 eV.

RESULTS AND DISCUSSION

Edge scans

To calibrate the incident x-ray energy, an energy scan was made through the U M_{IV} and M_V edges while detecting the U M fluorescence. For this measurement, the graphite monochromator was replaced by a wide-open proportional counter. Intense resonances called "white lines" were observed near the M_{IV} and M_V edges. These resonances correspond to transitions to an unfilled band

below the continuum. The width of the lines is the convolution of the incident-beam energy spread, the inner-shell hole width, and the width of the unfilled band. Detailed information about the density of states in the near-edge region is thus masked by the inner-shell width, which is ~ 4 eV.[3,4]

Emission spectra from M_{IV} and M_V holes

After the incident-beam energy calibration was established, the graphite monochromator was installed, and a proportional counter set to accept all the radiation passed by the graphite monochromator. In this mode, the monochromator had a FWHM bandpass of around 80 eV. The incident beam was then tuned 18 eV below the M_{IV} edge and the emission spectrum surveyed [Fig. 3(a)]. With the incident beam tuned ~ 60 eV above the M_{IV} edge, the emission spectrum was again measured [Fig. 3(b)]. By comparing lines arising with predominantly $M_V(3d \frac{5}{2})$ holes to lines arising when both M_{IV} and M_V holes are created, it is possible to identify the various
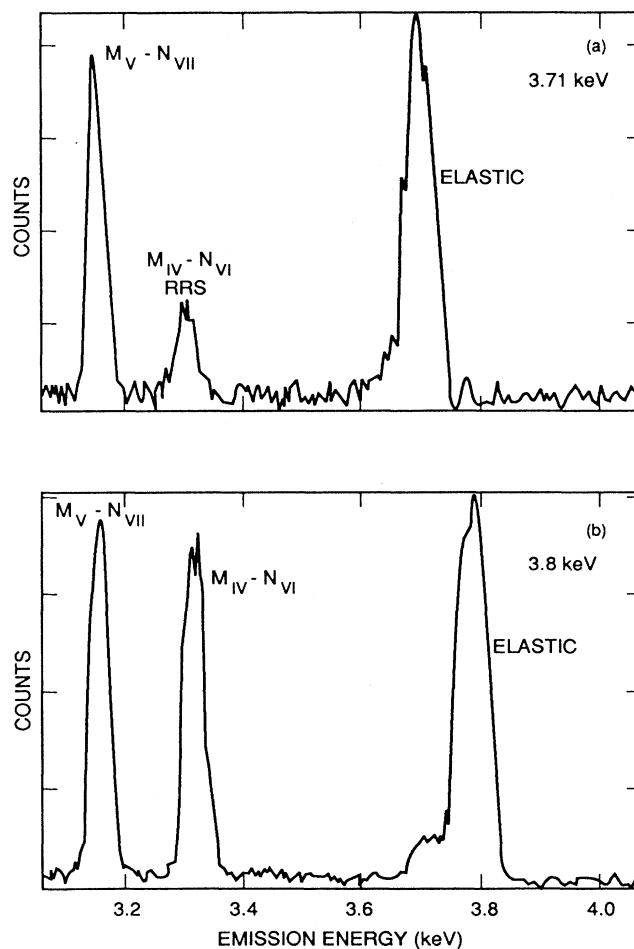

FIG. 3. Low-resolution M emission spectra (a) just below and (b) just above the U M_{IV} absorption edge.

transitions. This technique allows for an unambiguous assignment of the emission lines to a particular initial hole. Our assignment of lines agrees with that observed previously.[3-5]

High-resolution near-edge Raman spectra

The strongest lines observed were chosen for more careful study. These lines were the U $M_{IV}(3d\ \frac{3}{2})$-$N_{VI}(4f\ \frac{5}{2})$ and U M_V $(3d\ \frac{5}{2})$-$N_{VII}(4f\ \frac{7}{2})$. A linear sensitive gas proportional counter with better than 40 μ resolution[45] was installed at the parafocus of the graphite monochromator. The intensity distribution along the detector was collected by a multichannel analyzer. The energy scale of the detector was calibrated by observing the elastic scattering peak as a function of incident-beam energy. This calibration compared well with the estimated range and resolution of the graphite monochromator system. Additional confidence in the energy-scale calibration resulted from the unit slope observed in the dispersion of the resonant Raman peaks.

Because of the Gaussian energy bandpass of the graphite monochromator, the observed spectra are slightly distorted. The graphite monochromator was set to give optimal reflectivity for the pre-edge satellite line labeled A (Figs. 4 and 5). Away from the satellite, the spectrometer efficiency drops with a Gaussian distribution having a
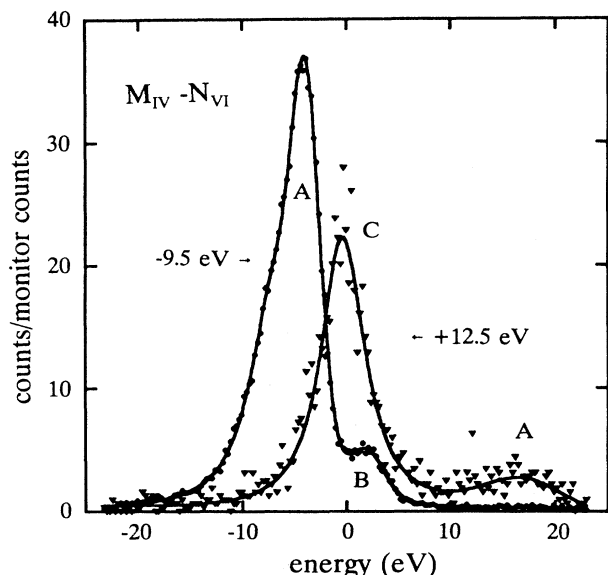
FIG. 4. Uranium M_{IV}-N_{VI} emission spectra taken near the U M_{IV} absorption edge. Spectra are shown for -9.5 and 12.5 eV relative to the nominal M_{IV} absorption edge. The data are normalized by the accumulated counts in an ion chamber monitor before the sample. The emission spectra go through a resonance between the incident x-ray energies plotted. The feature A is observed to be linearly dispersed with incident x-ray energy and is displaced to the right of the graph on the spectra taken 12.5 eV above the M_{IV} threshold. The small feature B observed -9.5 eV below threshold is also observed to be linearly dispersed with incident x-ray energy. Feature C appears very near resonance and has an energy almost independent of incident x-ray energy.
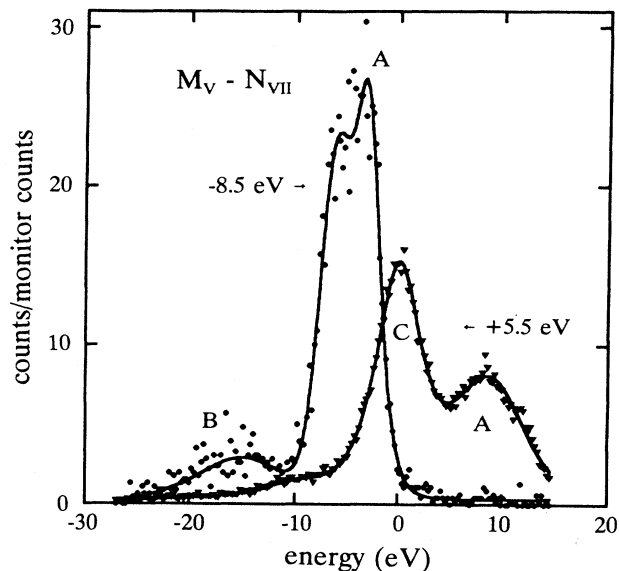
FIG. 5. Uranium M_V-N_{VII} emission spectra taken near the U M_V absorption edge. Spectra are shown for -8.5 and $+5.5$ eV relative to the nominal U M_V absorption edge. The data are normalized by the accumulated counts in an ion chamber monitor before the sample. The emission spectra peaks A and B go through a resonance between the incident x-ray energies plotted. The feature A is observed to be linearly dispersed with incident x-ray energy and is displaced to the right of the graph on the spectra taken 5.5 eV above the M_V threshold. The small feature B observed -8.5 eV below threshold is also observed to be linearly dispersed with incident x-ray energy. Feature C appears very near resonance and has an energy almost independent of incident x-ray energy.

FWHM of about 80 eV. The spectra covering ~ 40 eV are not corrected for this small bandpass distortion.

Typical spectra are illustrated in Figs. 4 and 5. At both the M_{IV} and the M_V edges, three distinct peaks were observed in the resonant Raman spectra. Well below the M_{IV} threshold, the M_{IV}-N_{VI} spectra are dominated by a sharp peak A, with a much smaller companion line B shifted by $+7$ eV. Both of these peaks are linearly dispersed with incident x-ray energy and have resonances about 4 eV below threshold (Fig. 6). The relative intensity of the high-energy companion line B is about 10% of A. Near and above threshold, a third peak C is observed. This peak has a nearly fixed position with incident energy above threshold. No high-energy companion is observed with peak C. Spectra were collected at ten different incident x-ray energies around the M_{IV} edge. The positions and intensities of the three peaks were determined by a nonlinear least-squares fit to the data using multiple Pearson VII functions and a sloping background. Pearson VII functions are used to describe symmetric peaks with shapes continuously variable between a Gaussian and a Lorenzian.[46] The asymmetric peak A was fit with two highly overlapping Pearson VII functions. The intensity and position of peak A was then estimated from the sum and weighted average of the two fitted peaks. Peaks B and C were fitted with single Pearson VII functions. Fits to the data above and below the

M_{IV} threshold are illustrated in Fig. 4. The intensity and emission energies of peaks A, B, and C are plotted as functions of incident x-ray energy minus the edge energy in Fig. 6.

Because of the threshold behavior of line C, and because it remains fixed in energy for x-ray energies above M_{IV} threshold, this line is identified as the M_{IV}-N_{VI} diagram line (usual fluorescent line). Above threshold we measure a line width of 3.8(2) eV, which is in good agreement with previous measurements of 3.9(2).[4] The resonant line A is identified as a so-called M_{IV}-N_{VI} spectator line associated with a pre-edge unfilled band.[26] For such spectator lines, the final state has an electron promoted to a pre-edge bound or band state, rather than to the continuum. The smaller line B is close to the position of the forbidden M_{IV}-N_{VII} line, shifted by the spectator shift. This line is puzzling, however, in that its energy shift lies outside of error bars for the M_{IV}-N_{VII} line, and because no M_{IV}-N_{VII} line has been observed in electron-excited spectra. We, therefore, speculate that this line arises from multiplet splitting due to the presence of the bound spectator electron.
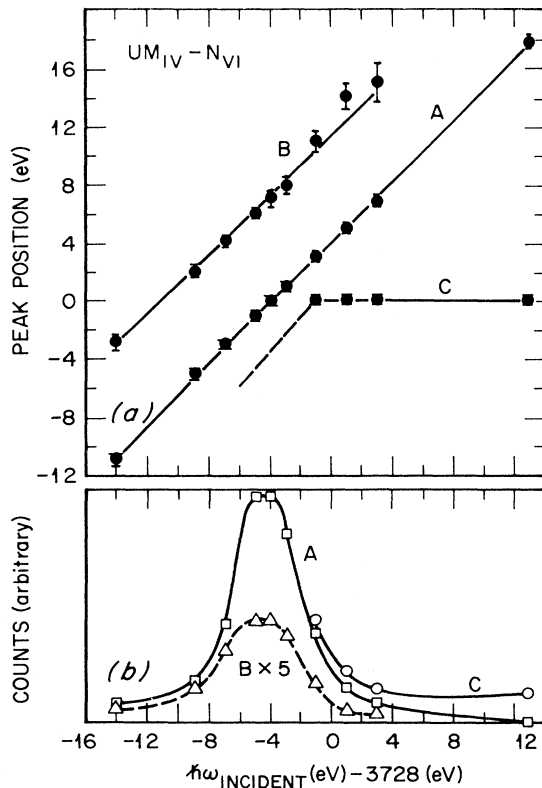
At the M_V edge, the M_V-N_{VII} line shows a similar splitting behavior, Fig. 5. Well below threshold the spectra have two peaks, which are linearly dispersed with energy. In this case, the low-energy companion B is about 10–15 % of the high-energy peak and shifted down in energy by 11 eV. Both peaks exhibit a resonance about 4 eV below threshold. The position of the low-energy companion B, relative to peak A, is very close to the splitting expected between the M_V-N_{VII} and the M_V-N_{VI} lines. The presence of an M_V-N_{VI} line has been detected previously,[3-5] but only at a level of 2.6% of the M_V-N_{VII} line. The relatively large spectator B peak is another indication of altered multiplet structure induced by the presence of a spectator electron. Again, a third peak appears near and above threshold and is identified as the diagram line. A small M_V-M_{VI} line is observed 10.5 eV below the diagram line (Fig. 5). This diagram M_V-M_{VI} line has the anticipated position but greater intensity relative to the diagram M_V-M_{VII} line than observed with electron-excited spectra. Data were not taken at sufficiently high energies to accurately measure the inner shell hole width of the M_V line. The spectator line A is observed to have
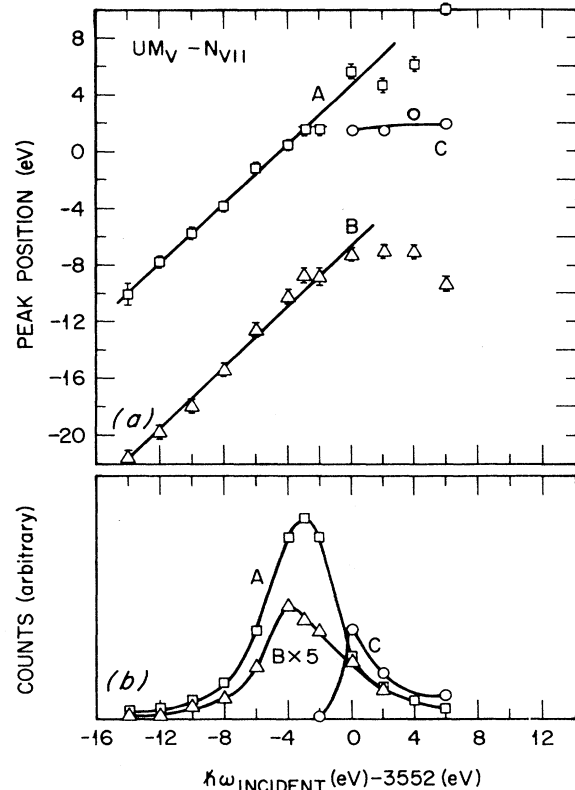

FIG. 6. (a) Peak position of the U M_{IV}-N_{VI} emission line as a function of incident x-ray energy near the U M_{IV} edge. Peak A is identified as a satellite peak corresponding to an electron promoted to a pre-edge band. Peak B is a companion to the pre-edge satellite peak A and has a resonance at the same incident x-ray energy. Peak C is the normal U M_{IV}-N_{VI} emission line observed when excited far above resonance. (b) Intensity of the U M_{IV}-N_{VI} emission lines as a function of incident x-ray energy near the U M_{IV} edge.

FIG. 7. (a) Peak position of the U M_V-N_{VII} emission lines as a function of incident x-ray energy near the U M_V edge. Peak A is identified as a satellite peak corresponding to an electron promoted to a pre-edge band. Peak B is a companion to the pre-edge satellite peak A (possibly M_V-M_{VI}) and has a resonance at the same incident x-ray energy. Peak C is identified as the diagram line. (b) Intensities of the U M_V-N_{VII} emission lines as a function of incident x-ray energy near the U M_V edge.

a "flat-top" shape over a wide range of incident x-ray energies. This shape was again fitted using two overlapping Pearson VII functions (Fig. 5). The fitted positions and intensities of the three peaks are plotted as a function of incident x-ray energy in Fig. 7.

Peak splitting behavior analogous to that observed here has been previously reported in resonant Auger studies of rare gases.[23-25] In these studies linearly dispersed peaks associated with unoccupied Rydberg levels were observed. These peaks were shifted relative to the diagram line by the energy difference between the continuum, and the Rydberg energy. This satellite was therefore labeled as a spectator satellite, since the excited electron acted energetically like a spectator. Although in the Auger spectra the diagram line is shifted, owing to the post-collision interaction effect,[47] the multiplet structure of the spectator line mimicked that of the diagram line. Here we detect a multiplet structure modified by the presence of the spectator electron. This complicates the study of the density of states, but reveals the strong correlation between the spectator electron in the pre-edge band and the core states. A possibly similar, although less dramatic effect, has been seen in near-edge x-ray emission for atomic argon. For argon the x-ray-emission line is seen to broaden near threshold and this has been ascribed to breaking of degeneracy due to the presence of a spectator electron.[48] Also in studies of molecules, the already split emission lines are observed to move relative to each other below threshold.[26]

Band shapes

The process of unraveling the band shape, to which the $3d(\frac{3}{2})$ and the $3d(\frac{5}{2})$ electrons are promoted, is complicated by the observed spectator splitting. Nevertheless, the resolution in this experiment is sufficient to detect differences at the two edges. It is clear even from the absorption measurements, that the $3d$ electrons can couple strongly to an unfilled band lying about 4 eV below the M_{IV} and M_V threshold energies. This gives rise to the intense white lines observed in absorption spectra. With absorption data these bands appear virtually identical, although there is a hint that at the M_{IV} edge the band is slightly separated from the continuum. Because of the intrinsic limited energy resolution imposed by the lifetime-broadened $3d$ hole width, it is unlikely that anything more can be learned from simple absorption measurements.

A more revealing indication of the band structure is given by Figs. 6 and 7, which show clearly that the spectator satellite line has a resonance about 4 eV below the nominal threshold. Because the transitions to this band are some seven times stronger than to the continuum, this band dominates the XRRS spectra below threshold. Particularly fascinating are differences in the below-threshold spectra shown in Figs. 4 and 5. The spectator satellite line at the M_{IV} edge has a sharp cutoff on the high-energy side, and a gradual low-energy cutoff. The spectator line at the M_V edge, however, appears to be flat topped, with sharp cutoffs at both the high- and low-energy edges.

A clearer picture of the near-edge density of unoccupied states can be obtained from the XRRS spectra by using Eq. (3) to remove the resonance dependence from the spectra. This process has no free parameters, since the resonance energy $E_{4f} - E_{3d}$ and the lifetime width Γ_{3d} are obtained from the emission spectra above threshold. Figures 8(a) and 8(b) show the spectra after removing the resonance contribution. In addition, we have inverted the energy dependence of the spectra so that the features
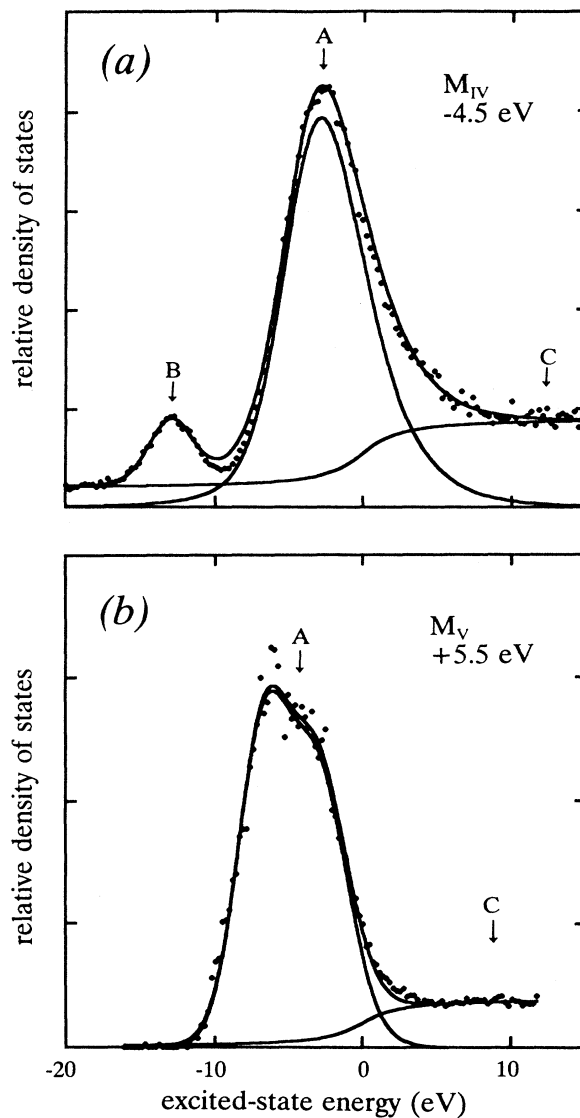

FIG. 8. (a) XRRS at the M_{IV} edge with the resonant product term removed and with the energy scale inverted to reflect $\eta(\epsilon_k)$. The pre-edge band labeled A is observed to be asymmetric and peaked. The continuum density of states labeled C is observed to be roughly flat above threshold. The small peak labeled B is an artifact arising from the additional emission line arising with a spectator electron. (b) XRRS at the M_V edge with the resonant product term removed, and with the energy scale inverted to reflect $\eta(\epsilon_k)$. The pre-edge band labeled B is flat topped.

correspond to the energy dependence of the density of states near threshold. The corrected spectra of Fig. 8 are typical for the M_{IV} and M_V edges and in the approximation of Eq. (3) are proportional to the unfilled density of states to which the $3d$ electron is promoted. The incident x-ray energies were chosen to reduce the size of the artifact due to the spectator emission peak B, and to optimize the statistics at the pre-edge unoccupied band. As can be seen, the spectra are similar but qualitatively different (Fig. 8). At the M_{IV} edge [Fig. 8(a)], the spectra show a peaked band with a much higher density of states than above threshold. The small feature 7 eV below the pre-edge band is an artifact from the "forbidden" spectator emission line (peak B). At the M_V edge the pre-edge band is more flat topped [Fig. 8(b)]. At both edges the data were fit to a simple model with a resolution-broadened step function representing the density of states in the continuum and with two overlapping Pearson VII functions to model the pre-edge band. An additional Pearson VII function was used to model the spectator artifact (feature B). The size and shape of the band feature A and the continuum C are roughly constant for various incident x-ray energies. However, the artifact feature B [Fig. 8(a)] corresponding to the spectator split B peak (Fig. 4) is not included in the model leading to Eq. (3). This peak grows away from the resonance condition and must be removed to correctly model the unfilled density of states.

The observed band structure is qualitatively similar to a feature observed in BIS measurements on URu_2Si_2.[49] The measurement presented here, however, indicates that the band density of states is at least six times higher than the density of states above threshold, whereas the BIS measurements show a difference of only a factor of two. This discrepancy is probably due to the fact that XRRS is less sensitive to transitions to d and s states and is sensitive only to the density of states near U atoms. Similarly, BIS measurements cannot distinguish between differences in the density of states for $5f(7/2)$ and $5f(5/2)$ electrons.

Why the $3d(\frac{3}{2})$ and $3d(\frac{5}{2})$ electrons should couple differently to the pre-edge band is not yet understood. A related effect has been observed in the L_{II} and L_{III} absorption edges of Pt.[50] A striking difference in the near edge structure of Pt L_{II} and Pt L_{III} has been ascribed to relativistic effects that cause the density of Pt $d(\frac{5}{2})$ and

$d(\frac{3}{2})$ to be different. The observed differences in the measured structure of the f-like band in U may arise from a similar relativistic influence on the density of states for $f(\frac{5}{2})$, compared to $f(\frac{7}{2})$. Alternatively, the different coupling of the $3d(\frac{3}{2})$ and $3d(\frac{5}{2})$ may be due to the fact that relativistically, the $3d(\frac{3}{2})$ is more p-like than the $3d(\frac{5}{2})$. This effect should be even more pronounced for $2p(\frac{1}{2})$, which becomes very s-like.

CONCLUSION

The uranium x-ray-emission spectra excited near the U M_{IV} and M_V edges has been measured with 1-eV resolution, revealing structure in the density of states near the edge. The XRRS spectra have been observed to split near threshold due to structure in the unoccupied density of states and due to core-hole spectator-electron interaction. After removing the resonant contribution to the emission spectra, the remaining difference at the M_{IV} and M_V edges reflects differences in how the $3d(\frac{3}{2})$ and $3d(\frac{5}{2})$ electrons couple to excited states. Theoretical work is now needed to explain the observed emission-line multiple structure with a spectator electron, and to explain apparent differences in the density of $5f(\frac{7}{2})$ states compared to that of $5f(\frac{5}{2})$ states. In addition to having very good signal to background compared to BIS, XRRS allows the study of transitions to states with specific symmetries. Although these experiments test the limits of current technology, the availability of third-generation synchrotron sources will allow orders-of-magnitude better counting statistics and, simultaneously, an order-of-magnitude better energy resolution in the near future.

[1]W. Stenstrom, dissertation, U. Lund, Sweden, 1919; E. Hjalmar, Z. Phys. **15**, 65 (1923); E. Lindberg, Nova Acta Regiae Soc. Sci. Ups. **7** (1931); W. C. Pierce and A. V. Grosse, Phys. Rev. **47**, 532 (1935).

[2]G. Lachere, C. R. Acad. Sci. **B267**, 821 (1968).

[3]O. Keski-Rahkonen and M. O. Krause, Phys. Rev. A **15**, 959 (1977).

[4]M. Ohno, A. Laakkonen, A. Vuoristo, and G. Graeffe, Phys. Scr. **34**, 146 (1986).

[5]H. Kleykamp, Z. Naturforsch. Teil A **36**, 1388 (1990).

[6]E. D. Isaacs, D. B. McWhan, C. Peters, G. E. Ice, D. P. Siddons, J. B. Hastings, C. Vettier, and O. Vogt, Phys. Rev. Lett.

62, 1671 (1989).

[7]J. P. Hannon, G. T. Trammell, M. Blume, and D. Gibbs, Phys. Rev. Lett. **61**, 1245 (1988).

[8]D. B. McWhan, C. Vettier, E. D. Isaacs, G. E. Ice, D. P. Siddons, J. B. Hastings, C. Peters, and O. Vogt, Phys. Rev. B **42**, 6007 (1990).

[9]E. D. Isaacs, D. B. McWhan, R. N. Kleinman, D. J. Bishop, G. E. Ice, P. Zschack, B. D. Gaulin, T. E. Mason, J. D. Garrett, and W. L. J. Buyers, Phys. Rev. Lett. **65**, 3185 (1990).

[10]T. E. Mason, B. D. Gaulin, J. D. Garrett, Z. Tun, W. J. L. Buyers, and E. D. Isaacs, Phys. Rev. Lett. **65**, 3189 (1990).

[11]K. Hamalainen, D. P. Siddons, J. B. Hastings, and L. E. Ber-

man, Phys. Rev. Lett. **67**, 2850 (1991).

[12]J. K. Lang and Y. Baer, Rev. Sci. Instrum. **50**, 221 (1979).

[13]T. Åberg, Phys. Scr. **21**, 495 (1980).

[14]T. Åberg and J. Tulkki, in *Physics of Atoms and Molecules*, edited by B. Crasemann (Plenum, New York, 1985), p. 419.

[15]C. J. Sparks, Phys. Rev. Lett. **33**, 262 (1974).

[16]Ph. Nozieres and E. Abrahams, Phys. Rev. B **10**, 3099 (1974).

[17]M. Gravilla and M. N. Tugulea, Rev. Roum. Phys. **20**, 209 (1975).

[18]Y. B. Bannett and I. Freund, Phys. Rev. Lett. **34**, 372 (1975).

[19]Y. B. Bannett, D. Rapaport, and Isaac Freund, Phys. Rev. A **16**, 2011 (1977).

[20]P. Eisenberger, P. M. Platzman, and H. Winick, Phys. Rev. Lett. **36**, 623 (1976), and references therein.

[21]P. Eisenberger, P. M. Platzman, and H. Winick, Phys. Rev. B **13**, 2377 (1976).

[22]P. Suortti, Phys. Status Solidi B **91**, 657 (1979).

[23]P. Suortti, Phys. Status Solidi B **92**, 259 (1979).

[24]A. F. Kodre and S. M. Shafroth, Phys. Rev. A **19**, 675 (1979).

[25]J. Tulkii and T. Åberg, Phys. Rev. A **27**, 3375 (1983).

[26]G. S. Brown, M. H. Chen, B. Crasemann, and G. E. Ice, Phys. Rev. Lett. **45**, 1937 (1980).

[27]G. E. Ice, G. S. Brown, G. B. Armen, M. H. Chen, B. Crasemann, J. Levin, and D. Mitchell, in *X-ray and Atomic Inner-Shell Physics*, Proceedings of the International Conference on X-ray and Atomic Inner-Shell Physics—1982, edited by B. Crasemann, AIP Conf. Proc. No. 94 (AIP, New York, 1982), p. 105.

[28]G. B. Armen, T. Åberg, J. C. Levin, B. Crasemann, G. E. Ice, and G. Brown, Phys. Rev. Lett. **54**, 1142 (1985).

[29]P. L. Cowan, Phys. Scr. **T31**, 117 (1990).

[30]P. L. Cowan, in *X-ray and Inner Shell Processes*, Proceedings of the International Conference on X-ray and Inner-Shell Process—1990, edited by T. A. Carlson, M. O. Krause, and S. T. Manson, AIP Conf. Proc. No. 215 (AIP, New York, 1990), p. 696.

[31]R. C. C. Perera, R. E. LaVilla, P. L. Cowan, T. Jach, and B. Karlin, Phys. Scr. **36**, 132 (1987); R. C. C. Perera, P. L. Cowan, D. W. Lindle, and R. E. LaVilla, J. Phys. (Paris) Colloq. **48**, C9-753 (1987).

[32]C. D. Caldwell, M. G. Flemming, M. O. Krause, P. Meulen, C. Pan, and A. Starace, Phys. Rev. A **41**, 542 (1990).

[33]S. B. Whitfield, C. D. Caldwell, M. O. Krause, Phys. Rev. A (to be published).

[34]J. J. Sakurai, *Advanced Quantum Mechanics* (Addison-Wesley, Reading, MA, 1967), Chap. 2.

[35]M. Blume, J. Appl. Phys. **57**, 3615 (1985).

[36]P. Eisenberger and P. M. Platzman, Phys. Rev. A **2**, 415 (1970).

[37]P. M. Platzman and P. A. Wolff, *Waves and Interactions in Solid State Plasmas* (Academic, New York, 1973).

[38]B. Ginatempo, P. J. Durham, and B. I. Gyorffy, J. Phys. Condens. Matter **1**, 6483 (1989).

[39]A. Habenschuss, G. E. Ice, C. J. Sparks, and R. Neiser, Nucl. Instrum. Methods **A266**, 215 (1988).

[40]G. E. Ice and C. J. Sparks, Nucl. Instrum. Methods **A291**, 394 (1988).

[41]G. E. Ice and C. J. Sparks, Nucl. Instrum. Methods **A291**, 110 (1990).

[42]J. B. Hastings, B. M. Kincaid, and P. Eisenberger, Nucl. Instrum. Methods **152**, 167 (1978).

[43]C. J. Sparks, G. E. Ice, J. Wong, B. W. Batterman, Nucl. Instrum. Methods **194**, 73 (1982).

[44]G. E. Ice and C. J. Sparks, Nucl. Instrum. Methods **A266**, 394 (1988).

[45]ORDELA, Inc. 139 Valley Court, Oak Ridge, Tennessee 37830.

[46]S. V. N. Naidu and C. R. Houska, J. Appl. Cryst. **15**, 190 (1982), and references therein.

[47]A. Niehaus and C. J. Zwakhals, J. Phys. B **16**, L135 (1983), and references therein.

[48]P. Cowan (private communication).

[49]J. W. Allen, J. S. Kang, Y. Lassailly, M. B. Maple, M. S. Torikachvilli, W. Ellis, B. Pate and I. Lindau, Solid State Commun. **61**, 183 (1987).

[50]R. J. Blake, in *X-ray Absorption Fine Structure*, Proceedings of the International Conference on X-ray Absorption Fine Structure—1990, edited by S. S. Hasnain, Series in Science and Technology, Ellis Horwood (Prentice-Hall, NJ, 1991), p. 21.